Oil-in-water emulsion separation

Fouling of alumina membranes with and without a silicon carbide deposition in constant flux filtration mode

Chen, Mingliang; Heijman, Sebastiaan G.J.; Luiten-Olieman, Mieke W.J.; Rietveld, Luuk C.

Important note
To cite this publication, please use the final published version (if applicable).
Please check the document version above.

Oil-in-water emulsion separation: Fouling of alumina membranes with and without a silicon carbide deposition in constant flux filtration mode

Mingliang Chen [a,*], Sebastiaan G.J. Heijman [a], Mieke W.J. Luiten-Olieman [b], Luuk C. Rietveld [a]

[a] Section of Sanitary Engineering, Department of Water Management, Faculty of Civil Engineering and Geosciences, Delft University of Technology, Stevinweg 1, 2628 CN Delft, The Netherlands
[b] Inorganic Membranes, MESA+ Institute for Nanotechnology, University of Twente, P.O. Box 217, 7500 AE Enschede, The Netherlands

ABSTRACT

Ceramic membranes have drawn increasing attention in oily wastewater treatment as an alternative to their traditional polymeric counterparts, yet persistent membrane fouling is still one of the largest challenges. Particularly, little is known about ceramic membrane fouling by oil-in-water (O/W) emulsions in constant flux filtration modes. In this study, the effects of emulsion chemistry (surfactant concentration, pH, salinity and Ca^{2+}) and operation parameters (permeate flux and filtration time) were comparatively evaluated for alumina and silicon carbide (SiC) deposited ceramic membranes, with different physicochemical surface properties. The original membranes were made of 100% alumina, while the same membranes were also deposited with a SiC layer to change the surface charge and hydrophilicity. The SiC-deposited membrane showed a lower reversible and irreversible fouling when permeate flux was below 110 L m^{-2} h^{-1}. In addition, it exhibited a higher permeance recovery after physical and chemical cleaning, as compared to the alumina membranes. Increasing sodium dodecyl sulfate (SDS) concentration in the feed decreased the fouling of both membranes, but to a higher extent in the alumina membranes. The fouling of both membranes could be reduced with increasing the pH of the emulsion due to the enhanced electrostatic repulsion between oil droplets and membrane surface. Because of the screening of surface charge in a high salinity solution (100 mM NaCl), only a small difference in irreversible fouling was observed for alumina and SiC-deposited membranes under these conditions. The presence of Ca^{2+} in the emulsion led to high irreversible fouling of both membranes, because of the compression of diffusion double layer and the interactions between Ca^{2+} and SDS. The low fouling tendency and/or high cleaning efficiency of the SiC-deposited membranes indicated their potential for oily wastewater treatment.

1. Introduction

Oily wastewater is becoming one of the major environmental concerns due to the large generated volumes, negative impacts on the aquatic environment, and potential threats to human health (Lin and Rutledge, 2018; Lin et al., 2019). Especially, emulsified oils in oil-in-water (O/W) emulsions are difficult to remove from a solution due to their small size (< 20 μm), and the high stability caused by the used surfactants, which considerably increase repulsive charge between oil droplets with a high zeta potential (Lu et al., 2016; Zhu et al., 2016).

Microfiltration (MF) and ultrafiltration (UF) have been widely studied to handle O/W emulsions, because of their distinct advantages over conventional methods, such as high flux, steady and good permeate quality, compact design, and small footprint (Chen et al., 2016; Ebrahimi et al., 2010; Hua et al., 2007). Ceramic membranes are gaining increasing attention for O/W emulsion separation as they have a narrow pore size distribution, a higher porosity, and higher hydrophilicity than polymeric membranes (Dong et al., 2019; Wang et al., 2022; Wu et al., 2022; Zhang et al., 2019). Therefore, better (reversible and irreversible) fouling control in water treatment has been observed than when polymeric membranes are used (Hofs et al., 2011; Nagasawa et al., 2020). Furthermore, ceramic membranes can potentially be cleaned with harsh chemicals and backwashed at high pressures, due to the high thermal, mechanical and chemical stability, for enhanced performance recovery, which can guarantee a longer service life (Eray et al., 2021; Nagasawa et al., 2020; Shi et al., 2022).

Still, fouling of the ceramic membranes is one of the major operational problems, as it increases the operational costs of the ceramic membranes during the filtration of O/W emulsions. It is generally acknowledged that membrane fouling is influenced by membrane properties, emulsion characteristics, and operational conditions (Lehman and Liu, 2009; Nagasawa et al., 2020). A hydrophilic membrane surface is supposed to be more permeable to water over hydrophobic oil droplets, thereby decreasing membrane fouling (Dickhout et al., 2017). In O/W emulsions, oil droplets are usually charged, positively or negatively, depending on the type and characteristic of the stabilizing surfactants. Therefore, electrostatic interactions between oil droplets and a charged membrane surface are assumed to play an important role in membrane fouling too. However, contrasting results regarding the role of electrostatic interaction have been reported. For example, in UF of O/W emulsions, stabilized by various types of surfactants, Matos et al. (2016) found that the negatively charged ZrO_2/TiO_2 ceramic membrane had a higher flux during filtration of an emulsion stabilized with an anionic surfactant. It was concluded that the electrostatic repulsion prevents the formation of a cake layer on the membrane surface and thus reduces the fouling. However, a lower flux was observed when filtering an emulsion stabilized with a cationic surfactant. A similar phenomenon was reported by Zhang et al. (2009), who found that a higher and more stable permeate flux was achieved for MF of an emulsion stabilized with sodium dodecyl sulfate (SDS, anionic), using a negatively charged TiO_2 doped Al_2O_3 membrane. In contrast, Lu et al. (2015) found that the TiO_2/ZrO_2 ceramic membranes had less irreversible fouling and a higher rejection of dissolved organics when challenged with O/W emulsions stabilized with an oppositely charged surfactant to the membrane. A synergetic steric effect and a demulsification effect were considered as the main reasons for the lower fouling due to the prevention of pore blockage.

Hence, there is no consensus in the currently available literature on whether electrostatic repulsion or electrostatic attraction plays a role in ceramic membrane fouling alleviation. The contradicting results on the effect of electrostatic interaction on membrane fouling may be explained by the differences in the feed characteristics, such as oil droplets size, surfactant concentration, and salinity. In addition, these studies were conducted at a constant pressure filtration mode, where a decline of permeate flux over time was observed. As a result, the observed fouling behavior is not only caused by the interaction between oil droplets and membrane surface but also due to the changing hydrodynamic environment and solute concentration near the membrane (Miller et al., 2014b). In practice, constant flux MF/UF filtration is preferred since the rate of permeate flow through the membrane's pores is more constant than in fixed TMP studies. The maintained constant hydrodynamic environment near the membrane surface favours the comparison of membrane fouling (Miller et al., 2014a, 2014b).

Therefore, this study is dedicated to a better understanding of the effect of surface charge of ceramic membranes on membrane fouling in constant flux filtration mode of an O/W emulsion stabilized with an anionic surfactant. Backwashing and multiple filtration cycles were performed in order to distinguish between hydraulic reversible and hydraulic irreversible fouling. SDS, a commonly used anionic surfactant, was employed to prepare negatively charged oil droplets. Al_2O_3 ceramic membrane and SiC-deposited ceramic membranes were selected, since both Al_2O_3 and SiC have a hydrophilic surface, but the isoelectric point (IEP) of these two materials is different. Al_2O_3 usually has a relatively high IEP (8–9), while a low IEP (2–3) has been found for SiC (Xu et al., 2020). Therefore, the surface charge of the two membranes would be opposite in a neutral environment, potentially leading to different fouling mechanisms. In addition, other factors like permeate flux, SDS concentration, pH, salinity, and Ca^{2+} concentration were investigated.

2. Materials and methods

2.1. Materials

Mineral oil (330760, Sigma-Aldrich), sodium chloride (NaCl) (99%, Baker Analyzed), calcium chloride dihydrate ($CaCl_2 \cdot 2H_2O$) (99%, Merck KGaA, Germany) and SDS (> 99%, Sigma-Aldrich) were used for the preparation of the O/W emulsion. HCl ($\geq$ 37%, Honeywell, Fluka™) and NaOH (0.1 M, Merck, Germany) were used for pH adjustment and membrane cleaning. Citric acid (99.9%, powder) was ordered from VWR International. All chemicals and solvents were used as received without further purification. Demineralized water (conductivity < 0.1 µs cm^{-1}), produced at WaterLab, TU Delft (water filtered by a reverse osmosis filter, a candle filter and a resin vessel), was used to prepare the aqueous solution and to rinse the filtration system and membrane samples.

2.2. Ceramic membranes

Commercial single-channel tubular ceramic Al_2O_3 membranes with a pore size of 100 nm were provided by CoorsTek Industry (the Netherlands) and commercial flat Al_2O_3 membranes were purchased from Inopor (Germany). The tubular membranes consist of a selective layer and a support layer both with α-Al_2O_3, having an inner diameter of 7 mm, an outer diameter of 10 mm and a length of 150 mm. The flat membranes have a pore size of 100 nm with a diameter of 100 mm and a thickness of 3 mm. The SiC-deposited membranes were prepared by low-pressure chemical vapor deposition (LPCVD), with Al_2O_3 tubes as support, at Else Kooi Lab, TU Delft. The Al_2O_3 tubes were deposited with a thin layer of amorphous SiC using two precursors (SiH_2Cl_2 and C_2H_2/H_2) at a temperature of 750 °C and pressure of 80 Pa (Morana et al., 2013). Three different deposition times (60, 90 and 120 min) were chosen to obtain SiC-deposited membranes with various pore sizes. More details on the preparation can be found in Chen et al. (2020a). The deposited SiC membranes are referred to as D60, D90, D120, corresponding to the deposition time of 60, 90 and 120 min, respectively. The pristine Al_2O_3 membranes are referred to as D0. The characteristics of the membranes are listed in Table 1. The flat disk membrane samples were deposited at the same conditions as used for the tubular ones for zeta potential measurements.

2.3. Membrane characterization

The surface charge of the membranes was characterized by the zeta potential with an electrokinetic analyser, SurPASS (Anton Paar, Graz, Austria). The instrument measures the streaming potential of the solid's surface and then the corresponding zeta potential is automatically calculated using the Helmholtz–Smoluchowski equation (Nagasawa et al., 2020). Potassium chloride (KCl, 5 mM) was used as the electrolyte solution, while the pH was adjusted by HCl (0.1 M) and NaOH (0.1 M). Before the test, the flat membrane discs were cut into a rectangular shape (20 × 10 mm) to match the module. The samples were measured in a range of pH values from 2 − 10 with a pH difference of 1 using an automated titration unit.

The water contact angle of the Al_2O_3 and SiC-deposited membranes

Table 1
Characteristics of the Al_2O_3 and SiC-deposited membranes.

Membrane label	Deposition time (min)	Selective layer	Pore size (nm)	Permeance (L m^{-2} h^{-1} bar^{-1})
D0	0	α-Al_2O_3	71[a]	350±10
D60	60	SiC	60	265±15
D90	90	SiC	54	220±20
D120	120	SiC	47	177±10

[a] the pore size measured with porometry is a little smaller than that (100 nm) provided by supplier.

were measured by a contact angle measurement (Dataphysics OCA20, Germany). The morphology of the ceramic membranes was characterized by a field emission scanning electron microscopy (SEM, FEI Nova Nano SEM 450, USA). The pore size distribution of the membranes was determined by capillary flow porometry (Porolux 500, IBFT GmbH, Germany). The surface roughness of the membranes was measured by atomic force microscopy (AFM) (Dimension Icon, Bruker, USA).

2.4. Oil-in-water emulsion

The O/W emulsions were prepared by adding 3 mL mineral oil to 2 L of demineralized water in the presence of SDS as the stabilizing agent. First, the emulsion was continuously stirred with a magnetic stirrer (L23, LABINCO, the Netherlands) at a speed of 1500 rpm for 36 h and then ultrasonicated (521, Bransonic, US) for 2 h until it appeared milky white. Afterwards, the emulsion was diluted to 6 L with a final oil concentration of 400 mg L^{-1} for filtration experiments. Four different SDS concentrations (33, 66, 100, 133 mg L^{-1}) were respectively used in order to study the effect of SDS concentration on membrane fouling. NaCl (1, 10, 100 mM) and Ca^{2+} (1 mM) were added into the emulsion with 100 mg L^{-1} SDS to study the effect of ionic strength and Ca^{2+} on membrane fouling, respectively. Each filtration run was finished on the same day to reduce the effect of oil droplet aggregates or coalescence. The pH of the emulsions was adjusted by HCl (0.1 M) and NaOH (0.1 M) and measured by a pH sensor (inoLab™ Multi 9420 - WTW). Electrical conductivity of the emulsion was measured by a multi-meter (inoLab™ Multi 9420 - WTW). The oil droplet size distribution and zeta potential were analyzed in triplicate with a particle size analyzer (Bluewave, Microtrac, USA) and a Malvern Zetasizer Nano ZS (Malvern Instruments Ltd., UK), respectively.

2.5. Fouling experiments with O/W emulsions

2.5.1. Constant flux crossflow fouling experiments

O/W emulsion filtration experiments were performed with a constant permeate flux crossflow fouling apparatus (Fig. 1), which has been described in detail in Chen et al. (2020a). The effective filtration area of each membrane module was 0.003 m^2. The concentrate valve was closed during filtration and the feed pump (DDA12–10, Grundfos, Denmark) has a controlled flow (measured and adjusted by the pump). A constant crossflow velocity of 0.44 m/s was provided by a circulation pump (VerderGear, Verder B.V., the Netherlands). Because the pressure at the permeate side was equal to atmospheric, the TMP was thus determined by the average of the inlet and outlet pressures on the two sides of the membrane module, which were monitored by two pressure transducers (GS4200-USB, ESI, UK). The pressures were continuously logged with a time interval of 30 s to the computer. During the filtration, the membrane was fouled and the membrane resistance increased, resulting in an increase in TMP.

2.5.2. Filtration protocol

The filtration experiments were conducted at room temperature (22 ± 3 °C). Before each filtration experiment, the system was thoroughly cleaned with demineralized water to remove residual chemicals and air. Afterwards, the initial water permeance of each membrane was measured at the same permeate fluxes as used for O/W filtration with demineralized water. The fouling experiment for each membrane consisted of several cycles which were dependent on the filtration conditions (permeate flux and emulsion chemistry). The filtration cycle was applicable for all membranes. Each cycle consisted of three phases: 1) Filtration at a specified flux for a pre-set time (Table 2), 2) Backwashing the membrane module with demineralized water at a fixed pressure of 3 bar for 30 s to remove hydraulically reversible fouling, 3) Forward flush with feed emulsion for 15 s to remove the backwash remaining liquids and replace the solution in the loop with the fresh feed.

Three permeate fluxes (90, 100, 110 L m^{-2} h^{-1}) were respectively used to compare the membrane performance based on the threshold flux of the membranes, because then the effect of membrane surface properties on fouling can be well studied (Luo et al., 2012) and the filtration time for each flux was chosen based on the same volume of permeate production. The filtration time per cycle has an effect on membrane fouling; therefore, two different filtration times were selected at a flux of 110 L m^{-2} h^{-1} for comparison. When challenged with the oil emulsion with high salinity or Ca^{2+} concentration, the permeate flux and filtration time were reduced as severe membrane fouling was observed Table 2. lists the characteristics of the O/W emulsion, the permeate flux and the

Table 2
Characteristics of the O/W emulsions, permeate flux and the corresponding filtration time per cycle for constant flux filtration experiments.

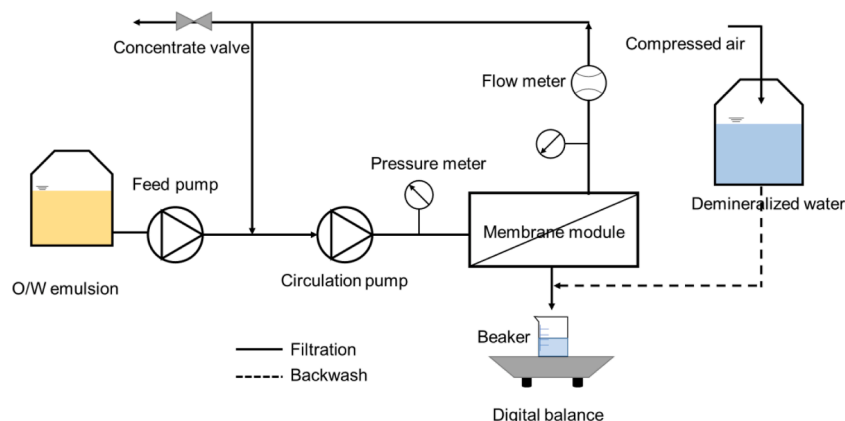| O/W emulsion					Permeate	Filtration
SDS (mg L^{-1})	pH	NaCl (mM)	Ca^{2+} (mM)	Conductivity (μs cm^{-1})	flux (L m^{-2} h^{-1})	time (min)
100	5.6	0	0	31	90	20
100	5.6	0	0	31	110	16
100	5.6	0	0	31	110	14
33	5.6	0	0	10	100	18
66	5.6	0	0	19	100	18
100	5.6	0	0	31	100	18
133	5.6	0	0	40	100	18
100	8	0	0	31	100	18
100	10	0	0	31	100	18
100	5.6	1	0	158	90	20
100	5.6	10	0	1305	60	12
100	5.6	100	0	11.58 ms cm^{-1}	50	10
100	5.6	1	1	352	50	10

Fig. 1. Schematic view of the constant flux crossflow filtration setup.

corresponding filtration time per cycle. A short filtration time was used as a faster fouling was observed with extended filtration time, leading to a decrease in the permeate flux (Fig. S1). In addition, in MF/UF, a filtration time of 15 min is common practice in full scale installations.

Between the various filtration runs, the membranes were first backwashed at 3 bar for 30 s and then they were chemically cleaned with a base solution by soaking them in a sodium hydroxide solution (0.01 M NaOH) for 1 h at 65 °C, followed by three times rinsing with demineralized water. Afterwards, the membranes were soaked in a citric acid solution (0.01 M) for another 1 h at 65 °C, as recommended in literature (Fraga et al., 2017; Zsirai et al., 2018). When the permeance of the membranes was not fully recovered after the chemical treatment, the membranes were heated at 200 °C for 2 h in a muffle furnace (Nabertherm Controller P 300, Germany). In this way, the membrane performance was completely recovered for the next filtration experiment.

In addition to the filtration experiments, where a constant flux was used during each run, flux-stepping experiments were carried out with D0 and D90 to determine the membrane threshold flux, as recommended in literature (He et al., 2017; Miller et al., 2014b). In this protocol, the permeate flux of the membrane was increased stepwise every 20 min from 40 to 80 L m^{-2} h^{-1} in an increment of 10 L m^{-2} h^{-1}. Then the flux was further increased by 10 L m^{-2} h^{-1} until a flux of 110 L m^{-2} h^{-1} was reached with reduced filtration times (Table S1), as rapid fouling was observed at these high fluxes. TMP was continuously monitored during each filtration interval.

2.5.3. Data analysis

The initial pressure for each membrane varied due to the permeance differences. In order to better compare the membrane performance, the permeance (*P*) of the membranes during filtration were normalized to the initial P_0, which was determined by the first value in the first cycle where the setting flux was reached.

The membrane resistance was calculated based on the resistance-in-series model (Chen et al., 2020a), as shown in Eq. (1):

$$R_t = \frac{TMP}{\mu J} = R_m + R_r + R_{ir} \tag{1}$$

where *J* is the membrane flux (m/s), *TMP* is the applied trans-membrane pressure (Pa), μ is the dynamic viscosity of the permeate (Pa·s), $R_t\,(m^{-1})$ represents the total resistance, which is consist of intrinsic membrane resistance (R_m), hydraulically reversible resistance (R_r), and irreversible unphysical removable resistance (R_{ir}). R_m was determined through the filtration of demineralized water and R_t was measured according to the final filtration pressure of each filtration cycle of O/W emulsion. The fouled membrane was backwashed with demineralized water under a pressure of 3 bar for 30 s and then R_r was measured. Therefore, the R_{ir} could be calculated from R_t - R_r - R_m.

The permeance recovery (R_p) of the membrane was determined by the following equation:

$$R_p = P/P_0 \times 100\% \tag{2}$$

where P_0 is the initial permeance of the clean membrane, *P* is the initial permeance of the fouled membrane after backwashing with demineralized water or cleaning with chemicals.

The methods used to determine membrane rejection and the results were provided in the supporting information (Fig. S2, S13 and S16).

3. Results and discussion

3.1. Characteristics of oil emulsion and membranes

Characteristics of O/W emulsions, prepared at various SDS concentrations, were evaluated in terms of zeta potential (Fig. 2a) and oil droplet size (Fig. S3). The O/W emulsions, stabilized with SDS, were negatively charged with a zeta potential ranging from −65 to −77 mV. The majority of the oil droplet sizes were in the range of 1 to 10 μm and a small amount of even smaller oil droplets (70–100 nm) was observed when the concentration of SDS reached 133 mg L^{-1} (Fig. S3). The zeta potential of the Al$_2$O$_3$ membrane was positive when the pH was lower than 6, while a negative surface charge was observed with a solution pH higher than 6 (Fig. 2b). Similar results were also reported by Nagasawa et al. (2020), although in the studies by Atallah et al. (2017) and Kosmulski (2011), the IEP of Al$_2$O$_3$ membranes was determined to be around 8 or 9. All SiC-deposited membranes had a negative surface charge in the investigated pH range (2–10). The zeta potentials of D90 and D120 were similar, but much lower than that of D0 and D60, possibly due to the thicker SiC layer on the sample surface with a longer deposition time (Yang et al., 2021). The results of other characteristics (pore size distribution, surface morphology, surface hydrophilicity and roughness) of the membranes are given in the supporting information (Fig. S4, S5, S6 and S7). Compared to the pristine Al$_2$O$_3$ membrane, the deposited membranes had a narrower pore size distribution and smaller average pore sizes.

3.2. Comparison of membrane fouling of the membranes

The Al$_2$O$_3$ membrane (D0) and the three SiC-deposited membranes (D60, D90 and D120) were compared for O/W emulsion filtration (in demineralized water) at a constant flux of 100 L m^{-2} h^{-1}, as shown in Fig. 3. The normalized permeance curve (see Fig. 3A) indicates that the pristine Al$_2$O$_3$ membrane without SiC deposition had the highest fouling tendency, despite that the fouling curves were similar for all studied membranes in the first two cycles. After the first filtration cycle, the permeance of all membranes was recovered suggesting little irreversible
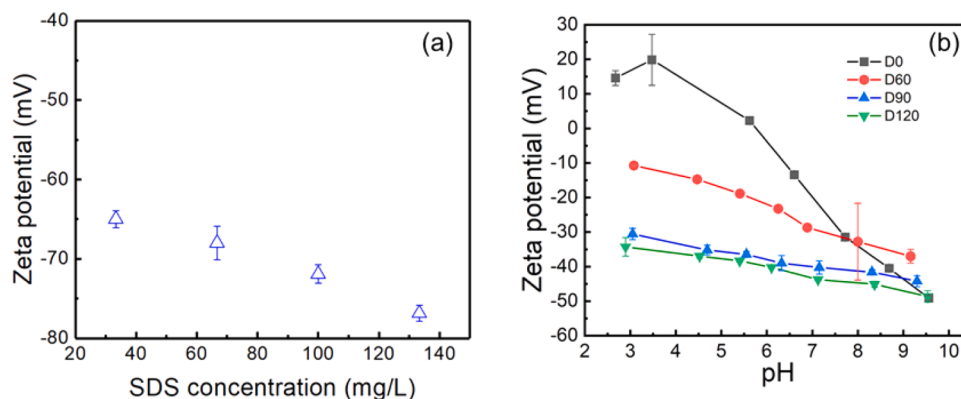

Fig. 2. (a) Zeta potential of O/W emulsion (0 mM NaCl) stabilized by SDS at different surfactant concentrations, and (b) zeta potential of Al$_2$O$_3$ membrane (D0) and SiC-deposited membranes (D60, D90 and D120). The conductivity of the O/W emulsion was given in Table 2.
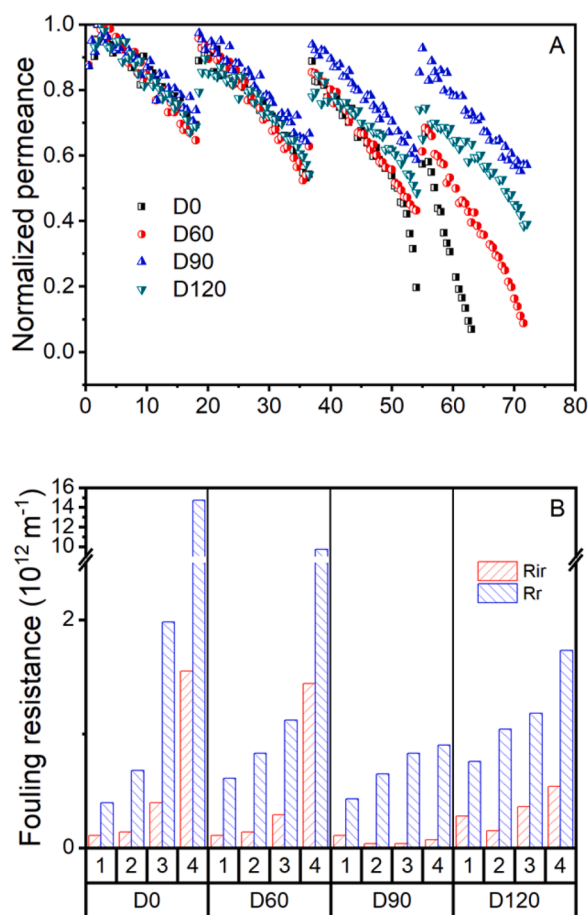
Fig. 3. Filtration of O/W emulsion (pH = 5.6, 400 mg L^{-1} oil and 66 mg L^{-1} SDS) at a constant flux of 100 L m^{-2} h^{-1} of four membranes (four filtration cycles): (A) normalized permeance, and (B) fouling resistance. In the fourth cycle, D0 was terminated after 9 min due to the rapid fouling.

fouling. However, with more filtration cycles, irreversible fouling in the membranes gradually increased, causing a loss of permeance. In the final filtration cycle, D90 showed the highest recovery of permeance (up to 94%) as compared to the other membranes.

The irreversible and reversible fouling was further evaluated by fouling resistance Fig. 3.B shows the fouling resistances of the four filtration cycles for all membranes. It can be observed that both the reversible and irreversible fouling were high for the Al$_2$O$_3$ membrane (D0) with a final R_r and R_{ir} of 14.7 × 10^{12} m^{-1} and 1.5 × 10^{12} m^{-1}, respectively. Deposition of a SiC layer at 60 min (D60) exhibited a minor influence on membrane fouling control as the final R_r and R_{ir} were still high. However, both the reversible and irreversible fouling were considerably alleviated for D90 and D120. Especially the fouling of D90, showing a final R_r and R_{ir} of 9 × 10^{11} m^{-1} and 0.7 × 10^{11} m^{-1}, was reduced by 93% and 95%, respectively, as compared with that of D0.

As shown in Fig. 2b, after deposition with a layer of SiC on the pristine Al$_2$O$_3$ membrane, the membrane surface charge was changed from positive to negative at a pH of 5.6. In addition, the surface hydrophilicity (Fig. S6) of the membranes was enhanced after the deposition, while the surface roughness was not affected as confirmed by SEM and AFM results (Fig. S5 and S7). As only a thin layer of SiC was deposited on the membrane surface of D60, the negative charge of surface was much lower than that of D90 and D120. Therefore, electrostatic repulsion between the D60 membrane and oil droplets was expected to be weaker, leading to more fouling (Yang et al., 2021).

The surface hydrophilicity, roughness and charge of D90 and D120 were similar (Fig. 2b, Fig. S6 and S7), but higher fouling was found in

D120 after four filtration cycles. This is most likely because of the smaller pore size and lower permeance of D120. Because fouling experiments were operated at constant flux, a lower water permeance of the modified membranes implies that filtration was operated at higher pressures, which is considered to be crucial for promoting fouling, especially at the initial filtration stage (Kouchaki Shalmani et al., 2020). A decrease in pore size of D120 would likely increase the local flux when the global permeate flux over the membrane filtration area was the same as with D90, resulting in higher velocities and higher drag forces acting on oil droplets during constant flux filtration, thereby increasing fouling (Kasemset et al., 2016; Miller et al., 2014b). Therefore, when membrane surface properties are similar, the membrane with a smaller pore size normally has a smaller permeance, leading to a higher fouling tendency in constant flux filtration experiments. Higher fouling was indeed observed for the least permeable membrane due to the deformation of oil droplets (Fig. S8 and S9), as also found during the studies of Fux and Ramon (2017), where a clear correlation was observed between the irreversible fouling and the degree of droplet deformation imaged by a confocal microscopy. Because a constant backwash pressure was used in the experiments, a higher backwash efficiency was found for membranes with higher permeance due to the higher backwash velocity, as also suggested by Vroman et al. (2020).

From the above results, it was concluded that D90 showed the best fouling control in SiC-deposited membranes. Therefore, D90 and D0 were further used to study the effects of permeate flux, SDS concentration, pH, salinity, and Ca^{2+} concentration on membrane performance in the following sections.

3.3. Effect of permeate flux

The threshold fluxes of the membrane D0 and D90 were 93 and 87 L m^{-2} h^{-1}, respectively, as determined by the flux-stepping methods (Fig. S10 and S11). Therefore, three different permeate fluxes (90, 100, 110 L m^{-2} h^{-1}), were compared to study their effect on membrane fouling. At the flux of 90 L m^{-2} h^{-1}, close to the threshold flux, fouling of the membranes is mainly determined by the foulant-membrane interaction. When the flux is above the threshold flux (100 and 110 L m^{-2} h^{-1}), foulant-membrane and foulant-deposited-foulant interactions can be investigated under this condition (Luo et al., 2012).

The effect of permeate flux on the filtration of the O/W emulsion with the SiC-deposited membrane (D90) and Al$_2$O$_3$ membrane (D0) is shown in Fig. 4. At a flux of 90 L m^{-2} h^{-1}, some fouling was observed in both membranes as permeance declined with time. The normalized permeance curves of the two membranes were parallel and overlapped in the first two cycles, indicating that reversible fouling was similar. With more filtration cycles, the permeance curves of D0 shifted down which was not observed in D90, suggesting that irreversible fouling happened in D0 (Fig. 4a). When the permeate flux increased from 90 to 100 L m^{-2} h^{-1}, irreversible fouling became larger for both D0 and D90, as observed by lower initial normalized permeance of each cycle. The normalized permeance (84% recovery) of D90 was still higher than that (64% recovery) of D0 in the final cycle at the flux of 100 L m^{-2} h^{-1}.

During fouling experiments, higher fluxes bring larger amounts of emulsified oil foulants per time unit to the membrane surface, increasing foulant accumulation on the membrane (Miller et al., 2014a, 2014b). On the other hand, higher fluxes cause a stronger drag force acting on oil droplets, which, consequently lead to the deformation and coalescence of attached droplets and squeezing of oil droplets across the membrane pores, resulting in irreversible fouling of the membrane (Fig. 4d) (Chen et al., 2020b; Tummons et al., 2017). As shown in Fig. 4c, with a further increase in the flux to 110 L m^{-2} h^{-1}, a much higher irreversible fouling was observed in D90, compared to the lower fluxes, and close to that of D0. At this high flux, oil coalescence and internal fouling are more likely to occur, and therefore hydraulic cleaning became ineffective to remove the oil film (Zhu et al., 2017).

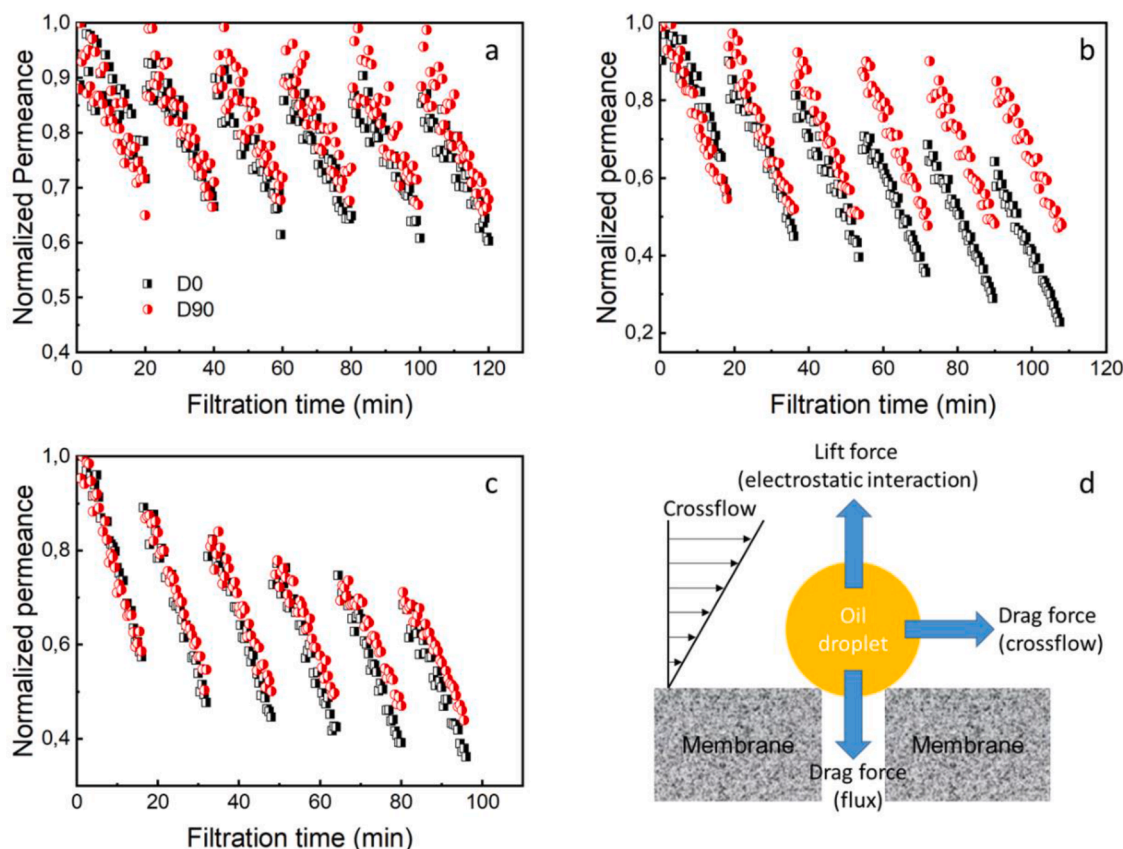When the water production during a filtration cycle was the same at

Fig. 4. Normalized permeance of D0 (black) and D90 (red) compared at various fluxes: (a) 90 L m^{-2} h^{-1}, (b) 100 L m^{-2} h^{-1}, and (c) 110 L m^{-2} h^{-1}. (d) Force balance on an oil droplet in crossflow filtration. The O/W emulsion has a pH of 5.6, oil concentration is 400 mg L^{-1} and the SDS is 100 mg L^{-1}.

the three studied fluxes, lower fouling was observed at a lower flux. However, further shortening the filtration time to 14 min per cycle at the highest flux (110 L m^{-2} h^{-1}) could control the fouling, especially for SiC-deposited membrane (Fig. S12). In this case, permeance recovery of SiC-deposited membrane increased from 71% to 94%, which was higher than that (84%) of the Al$_2$O$_3$ membrane.

3.4. Effect of SDS concentration

The effect of SDS concentration on fouling of the Al$_2$O$_3$ membrane (D0) and SiC-deposited membrane (D90) is shown in Fig. 5. At a low concentration of SDS (33 mg L^{-1}), the fouling of D90 was much less than that of D0, which can be observed by terminal normalized permeance and the recovery of the permeance of each cycle (Fig. 5a). The higher (ir) reversible fouling of D0 was attributed to the lack of electrostatic repulsion between the membrane and oil droplets. Increasing the concentration of SDS in the feed had a positive effect on the fouling of both

membranes, especially on the D0. As observed in Fig. 5b, the permeance recovery in the final cycle of D0 and D90 increased from 61% to 70% and from 81% to 87%, when the concentration of SDS was increased from 33 to 100 mg L^{-1}, respectively. With a further increase in the SDS concentration in the feed to 133 mg L^{-1}, the fouling difference between D0 and D90 was further reduced, with a permeance recovery of 81% and 90% in the final cycle, respectively. Similar results were reported by Virga et al. (2020), who found that less flux decline was observed for MF of an SDS stabilized O/W emulsion with a commercial SiC membrane, when SDS concentration increased from 0.1 to 1 times the critical micelle concentration (CMC). As SDS concentration was high (up to the CMC), O/W interfacial tension was considerably decreased, potentially leading to oil permeation through the membrane rather than accumulating on the membrane surface or in the pores. As a result, a higher permeate flux was observed. However, this mechanism cannot explain the results observed in our work, as the highest used SDS concentration (133 mg L^{-1}) was less than 0.06 times the CMC. In addition, no
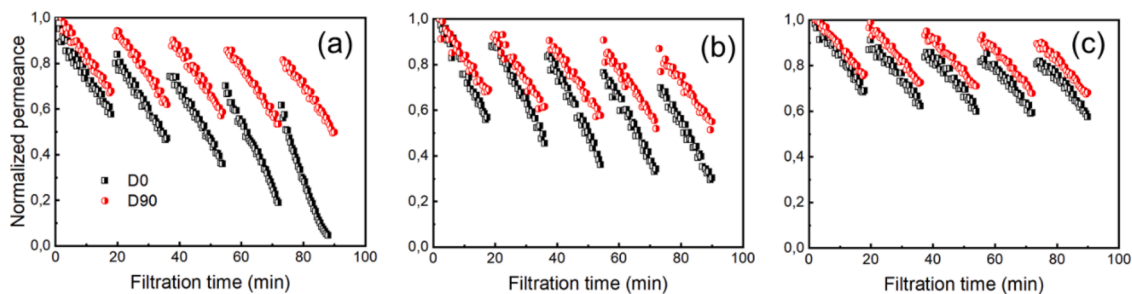

Fig. 5. Normalized permeance of D0 and D90 compared at various SDS concentrations: (a) 33 mg L^{-1}, (b) 100 mg L^{-1}, and (c) 133 mg L^{-1}. The filtration experiments were conducted at the flux of 100 L m^{-2} h^{-1}, O/W emulsion has a pH of 5.6, and the oil concentration is 400 mg L^{-1}.

variations in oil rejection were observed for emulsions stabilized with different SDS concentrations (Fig. S13).

The reversible and irreversible fouling of D0 and D90 was also evaluated by the fouling resistances (Fig. S14). The R_r and R_{ir} of D0 were considerably decreased, from $46 \times 10^{12}\,m^{-1}$ to $1.53 \times 10^{12}\,m^{-1}$ and from $3.57 \times 10^{12}\,m^{-1}$ to $0.7 \times 10^{12}\,m^{-1}$, respectively, when the concentration of SDS was increased from 33 to 133 mgL^{-1}. However, the R_r and R_{ir} of D90 were only slightly decreased, from $3.1 \times 10^{12}\,m^{-1}$ to $1.2 \times 10^{12}\,m^{-1}$ and from $0.95 \times 10^{12}\,m^{-1}$ to $0.4 \times 10^{12}\,m^{-1}$, respectively.

The SiC-deposited membrane was negatively charged while the Al$_2$O$_3$ membrane had a positive surface charge at a pH of 5.6 (Fig. 2b). A higher negative charge of the emulsion was observed with increasing SDS concentration, as determined with the zeta potential of the emulsions, prepared with various SDS concentrations (Fig. 2a). According to the adsorption model proposed by Gu and Zhu (1990), the adsorption of surfactant at the liquid/solid surface takes place in two steps. In the first step, the head groups of surfactant monomers preferably adhere to the hydrophilic membrane surfaces to form the first layer. Subsequently, a second layer is adsorbed on the first one (Nguyen et al., 2015). In addition, a slight decline of permeance of the Al$_2$O$_3$ membrane was observed for SDS solution filtration, indicating that SDS was adsorbed on the Al$_2$O$_3$ membrane. However, no adsorption of SDS on the SiC-deposited ceramic membranes was observed as the permeance maintained constant (Fig. S15). Therefore, the following fouling mechanism was proposed and is schematically shown in Fig. 6. At a low SDS concentration (33 mg L^{-1}), most of the surfactants were used to stabilize the oil droplets, leaving a low concentration of free SDS monomers in the solution. The negatively charged head of the SDS (and hydrophilic) will be attached to the positively charged Al$_2$O$_3$ membrane surface due to electrostatic attraction, leaving the hydrophobic tails towards the bulk

phase (Dobson et al., 2000). This forms a hydrophobic surfactant monolayer on the surface and therefore increases the fouling of D0 (Fernández et al., 2005; Matos et al., 2016). Increasing the SDS concentration, however, will result in a higher concentration of free surfactant monomers in the solution, and probably a new monolayer is formed on top of the pre-covered single monolayer on the membrane surface. In this case, the hydrophilic head (and negatively charged) of SDS is oriented towards the bulk phase as a result of hydrophobic interactions. Thus, the surface charge of the Al$_2$O$_3$ membrane is reversed from positive to negative (and again hydrophilic), which prevents the adsorption of oil droplets and alleviates the membrane fouling. The charge inversion of the membrane by surfactant has also been reported by Trinh et al. (2019), who found that surfactant-soaked membranes had the same charge as the surfactant-stabilized emulsion regardless of the surfactant type. However, surfactants and oil droplets can be hardly adsorbed on the membrane surface and in the membrane pores of the SiC-deposited membranes due to electrostatic repulsion (Lin and Rutledge, 2018; Zhang et al., 2009). The slightly improved fouling resistance of the SiC-deposited membranes can be ascribed to the enhanced electrostatic repulsion between the membrane and oil droplets with increased SDS concentration in the feed.

3.5. Effect of pH

To determine the effect of pH on membrane fouling, filtration experiments were conducted at three different pH values (Fig. 7). We chose pH 5.6 as the starting point to study the fouling of the two membranes as it is the native pH of the fresh O/W emulsion. In addition, this pH is commonly observed in oily wastewater (Wenzlick and Siefert, 2020). In all cases, the fouling was less in the SiC-deposited membrane than in the
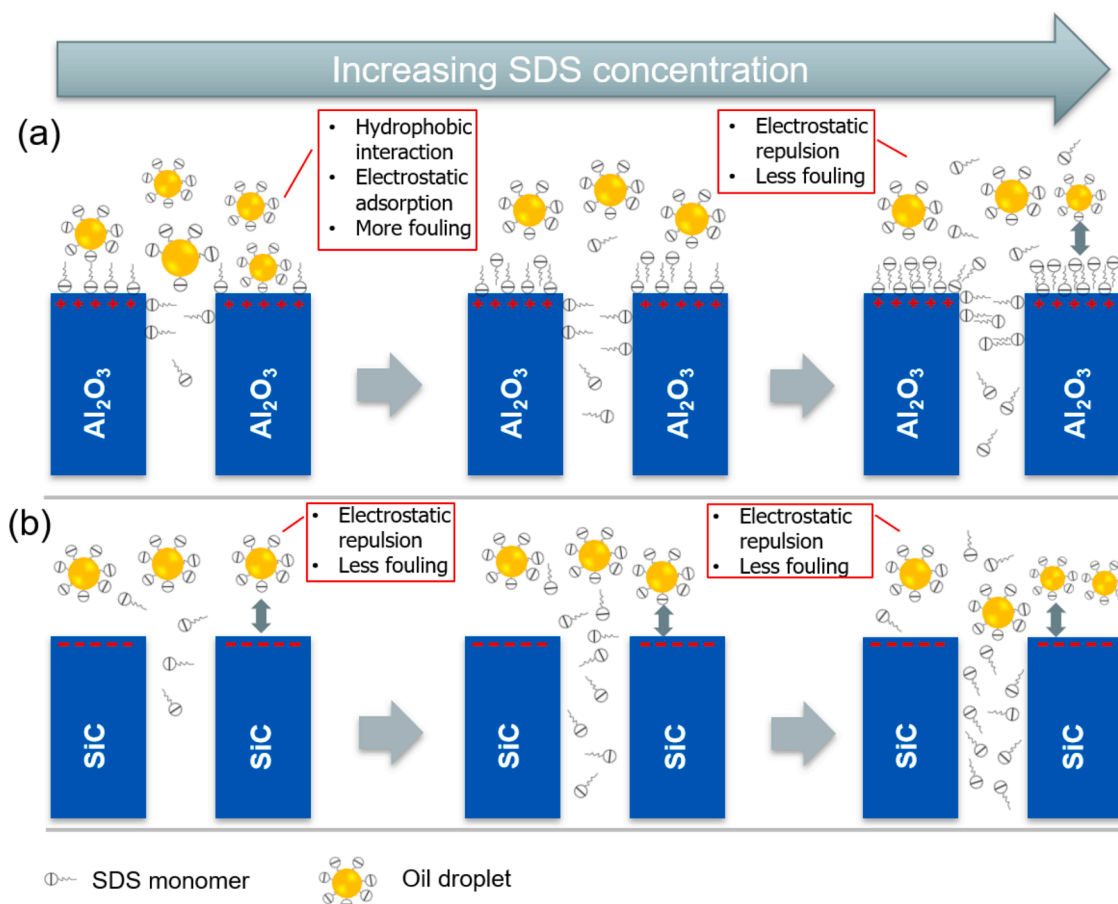

Fig. 6. Proposed fouling mechanism of (a) Al$_2$O$_3$ and (b) SiC membranes during filtration of SDS stabilized O/W emulsions at various SDS concentrations.
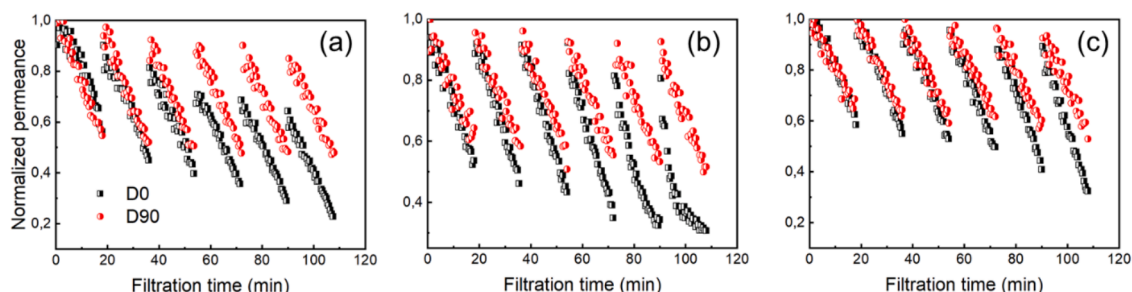
Fig. 7. Normalized permeance of D0 and D90 compared at various pH: (a) pH = 5.6, (b) pH = 8, and (c) pH = 10. The filtration experiments were conducted at the constant flux of 100 L m^{-2} h^{-1}, oil concentration is 400 mg L^{-1} and the SDS is 100 mg L^{-1}.

Al$_2$O$_3$ membrane. In addition, both membranes experienced a decrease of fouling with an increase in pH. Specifically, the normalized initial permeance of D0 and D90 in the final filtration cycle increased from 64% to 89%, and 85% to 93%, when pH increased from 5.6 to 10, respectively. This pH dependency can be attributed to the fact that, as pH increases, the surface charge of the membrane becomes more negative (Zhang et al., 2009). As shown in Fig. 2a, the zeta potential of the SiC-deposited membrane (D90) decreased from −37 mv to −44 mv with an increase in pH from 5.6 to 10, respectively. Consequently, the membrane surface was less prone to be fouled by the negatively charged oil droplets due to the stronger electrostatic repulsion. However, the surface charge of the Al$_2$O$_3$ membrane was positive at a pH of 5.6, and therefore more fouling was observed as it favourably interacted with the negatively charged solutes. The positively charged (+8 mv) surface was changed into negative (−49 mv) when filtering the feed with a pH of 10, and, therefore, electrostatic interaction became repulsive and contributed to decreased fouling (Abadikhah et al., 2018; Lee and Kim, 2014).

Although the zeta potentials of Al$_2$O$_3$ and SiC-deposited membranes were similar at a pH of 10, the fouling of the SiC-deposited membrane was still lower than that of the Al$_2$O$_3$ membrane. This can possibly be ascribed to the stronger hydrophilic surface of the SiC-deposited membrane (water contact angle = 0°) than that of the Al$_2$O$_3$ membrane (water contact angle = 25°) (Fig. S6). Xu et al. (2020) also compared the fouling of Al$_2$O$_3$ and SiC hollow fiber membranes for MF of O/W emulsions, a higher flux was observed for the more hydrophilic SiC membrane.

3.6. Effect of salinity and Ca^{2+}

It has been reported that the surface charge of oil emulsions and membranes decreases with the concentration of NaCl due to the compressed electrical double layer (He et al., 2017; Tanudjaja et al., 2017). Although the droplet size of oil was not changed with the salinity (Fig. S3), as shown in Fig. 8, the fouling of both D0 and D90 became
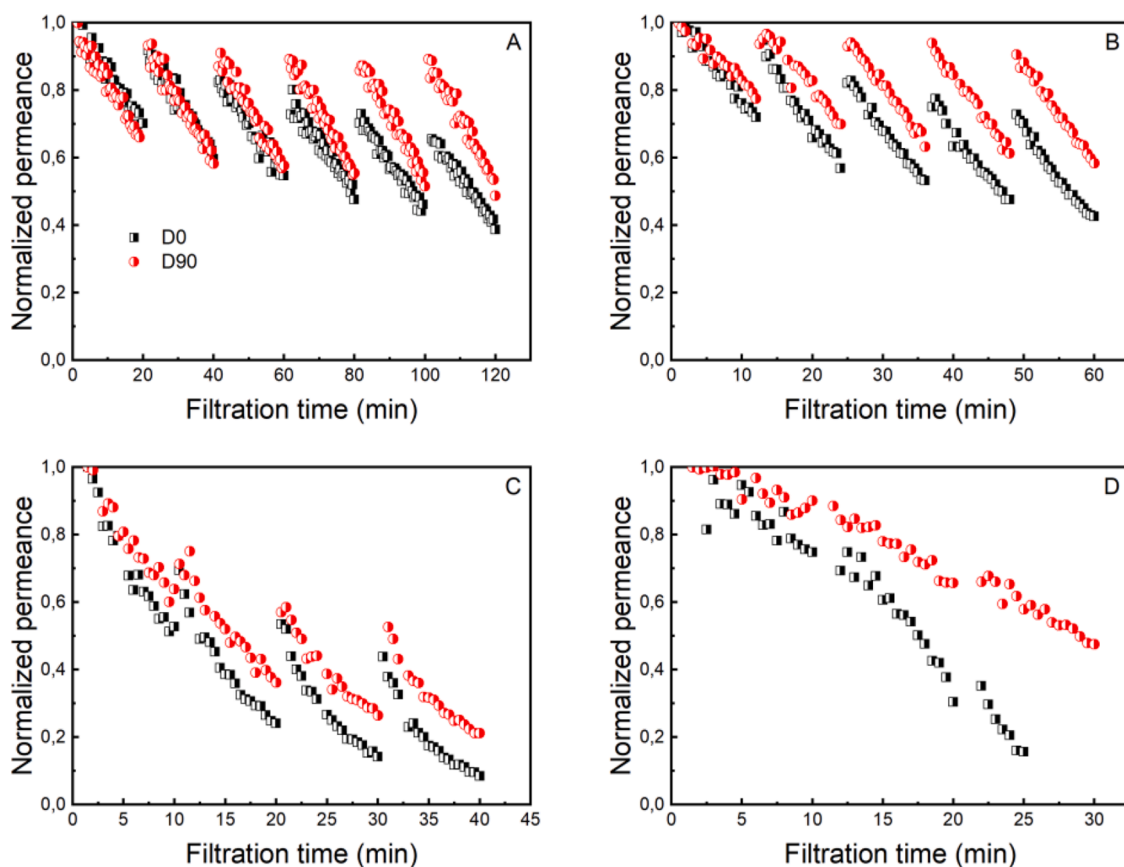

Fig. 8. Normalized permeance of D0 and D90 compared at various concentrations of NaCl and 1 mM Ca^{2+}: (A) 1 mM NaCl, (B) 10 mM NaCl, (C) 100 mM NaCl and (D) 1 mM NaCl + 1 mM Ca^{2+}. The emulsion has an oil concentration of 400 mg L^{-1}, pH of 5.6 and the SDS of 100 mg L^{-1}.

higher when NaCl concentration increased from 1 mM to 100 mM. However, the fouling of D90 was much lower than that of D0 when NaCl concentration was lower or equal to 10 mM. This indicates that the surface charge of the SiC-deposited membrane still had an effect on the fouling by oily wastewater with relatively low salinity, whereas, much more fouling was observed for both membranes when NaCl concentration reached 100 mM. At that salinity (100 mM NaCl), the flux recovery of D90 was close to that of D0, suggesting that irreversible fouling of the two membranes were similar. Probably, because, oil droplets were not easily lifted off the membrane with backwash, due to charge screening and an increase of cake layer density (Dickhout et al., 2019; He and Vidic, 2016).

Divalent cations such as Ca^{2+} and Mg^{2+} can also be present in oily wastewater. Their presence may accelerate membrane fouling due to more compression of the diffusion double layer compared to monovalent ions (Dickhout et al., 2017). As shown in Fig. 8D, the membrane fouling was worse when 1 mM Ca^{2+} was added to the emulsions and the backwashing was not effective anymore to restore the permeance. Therefore, the irreversible fouling was considered to be the main contributor to the membrane fouling. This can be explained by two effects of Ca^{2+} in the emulsion: (1) lower electrostatic charge of oil droplets and membranes are to be expected due to a compressed electrostatic layer when Ca^{2+} is present in the emulsion (Hong and Elimelech, 1997). Therefore, droplet coalescence on the membrane surface is promoted leading to a less permeable cake layer (Tummons et al., 2017); (2) SDS can interact with divalent Ca^{2+}, which may cause the formation of a complex between Ca^{2+} and the sulfate group of SDS (Panpanit et al., 2000; Sammalkorpi et al., 2009). As a result, less SDS molecules exist in the emulsion, as confirmed by permeate COD (Fig. S16), leading to a higher irreversible fouling of the membranes (Virga et al., 2020). However, the irreversible fouling of D90 was still lower than that of D0, even though the electrostatic repulsion became weaker. Tummons et al. (2017) studied the effect of Mg^{2+} on the fouling of an Al_2O_3 UF membrane by SDS stabilized emulsions. The presence of Mg^{2+} (6.7 mM) in the emulsion was observed to promote the coalescence of oil droplets on the membrane surface, leading to a higher flux decline of the membrane due to the less porosity of the cake layer. When the Mg^{2+} concentration was sufficiently high (42.6 mM), attached oil droplets coalesced to reach a critical size, which can probably be removed by crossflow to minimize the fouling in the constant pressure filtration condition.

3.7. Membrane cleaning efficiency

After filtration of O/W emulsions at high fluxes during multiple cycles, accumulation of irreversible fouling in membranes was inevitable. The permeance recovery of D0 and D90 were compared after backwashing, after NaOH (0.01 M) and after citric acid (0.01 M) cleaning (Fig. 9). The efficiency of backwashing was investigated after six cycles of filtration at a flux of 110 L m^{-2} h^{-1}, as was previously shown in Fig. 3c. The permeance recovery after backwashing of D90 (64%) was higher than that of D0 (45%), probably due to less sticky fouling in the membrane and to a more efficient backwashing. After soaking the membranes in NaOH (0.01 M) solution at 65 °C for 1 h, the permeance recovery of D0 and D90 reached up to 80% and 84%, respectively. The permeance of D90 could be further recovered to 98% after citric acid (0.01 M, 65 °C) treatment for 1 h, while the permeance of D0 could only be recovered to 84%. A high permeance recovery (100%) was also observed by Fraga et al. (2017) when using both acid and alkaline solutions to clean SiC membranes at 60 ± 5 °C after filtration of oily wastewater. However, the permeance recovery of D90 was lower, but still higher than that of D0, after filtration of O/W emulsions with either high salinity (100 mM NaCl) or the presence of Ca^{2+} (Fig. S17).

4. Conclusion

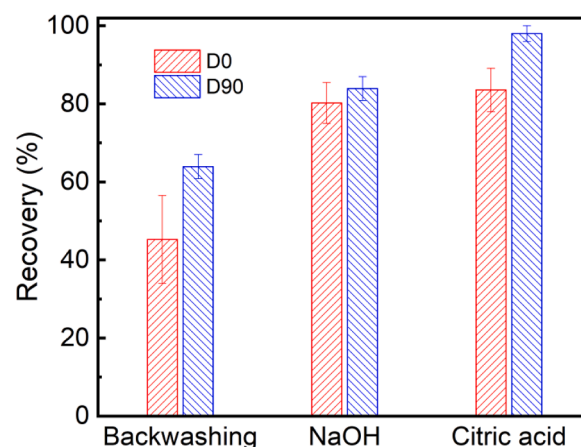The performance of Al_2O_3 and SiC-deposited ceramic membranes

Fig. 9. Permeance recovery of D0 and D90 with backwashing (3 bar/30 s), NaOH (0.01 M, 65 °C) cleaning and citric acid (0.01 M, 65 °C) cleaning. The membranes were fouled after 6 cycles of O/W emulsion filtration at a constant flux of 110 L m^{-2} h^{-1}, oil concentration of 400 mg L^{-1} and pH of 5.6.

was systematically compared during constant flux filtration of O/W emulsion with multiple filtration cycles. Both the operation and solution chemistry parameters affected the membrane fouling, while the extents varied, depending on the emulsion characteristics and operational parameters. The following conclusions were drawn:

(1) SiC-deposited membranes had a lower reversible and irreversible fouling than Al_2O_3 membranes, when, in multiple filtration cycles, the permeate flux was smaller or equal to 100 L m^{-2} h^{-1}. The fouling of both membranes was similar when the flux reached to 110 L m^{-2} h^{-1}.

(2) Increasing the concentration of SDS in the feed decreased fouling of both membranes, and a larger effect was observed for the Al_2O_3 membrane. The improved fouling resistance of the Al_2O_3 membrane can be ascribed to the effect of surfactant adsorption and charge inversion, while the enhanced electrostatic repulsion between the membrane and oil droplets was responsible for the lower fouling of the SiC-deposited membrane.

(3) The fouling of both Al_2O_3 and SiC-deposited membranes was reduced with increased pH due to the more negative zeta potential of the membrane surface and thus a stronger electrostatic repulsion.

(4) The fouling of the SiC-deposited membrane was less with a low salinity emulsion (1 and 10 mM NaCl), while only a small difference in irreversible fouling was observed for Al_2O_3 and SiC-deposited membranes for high salinity emulsions (100 mM NaCl) due to charge screening effect.

(5) The presence of a low concentration of Ca^{2+} (1 mM) in the emulsion led to high irreversible fouling for both membranes.

(6) The chemical cleaning efficiency of the SiC-deposited membrane was higher than that of the Al_2O_3 membrane.

Declaration of Competing Interest

The authors declare that they have no known competing financial interests or personal relationships that could have appeared to influence the work reported in this paper.

The Netherlands) for her help on language and grammar issues of the manuscript. Bob Siemerink, and Iske Achterhuis from Twente University are acknowledged for the support concerning the zeta potential measurements. Guangze Qin is acknowledged for measuring the membrane water permeance.

Supplementary materials

Supplementary material associated with this article can be found, in the online version, at doi:10.1016/j.watres.2022.118267.

References

Abadikhah, H., Zou, C.-N., Hao, Y.-Z., Wang, J.-W., Lin, L., Khan, S.A., Xu, X., Chen, C.-S., Agathopoulos, S., 2018. Application of asymmetric Si₃N₄ hollow fiber membrane for cross-flow microfiltration of oily waste water. J. Eur. Ceram. Soc. 38 (13), 4384–4394.

Atallah, C., Tremblay, A.Y., Mortazavi, S., 2017. Silane surface modified ceramic membranes for the treatment and recycling of SAGD produced water. J. Petrol. Sci. Eng. 157, 349–358.

Chen, M., Shang, R., Sberna, P.M., Luiten-Olieman, M.W.J., Rietveld, L.C., Heijman, S.G. J., 2020a. Highly permeable silicon carbide-alumina ultrafiltration membranes for oil-in-water filtration produced with low-pressure chemical vapor deposition. Sep. Purif. Technol. 253, 117496.

Chen, M., Zhu, L., Chen, J., Yang, F., Tang, C.Y., Guiver, M.D., Dong, Y., 2020b. Spinel-based ceramic membranes coupling solid sludge recycling with oily wastewater treatment. Water Res 169, 115180.

Chen, M.L., Zhu, L., Dong, Y.C., Li, L.L., Liu, J., 2016. Waste-to-resource strategy to fabricate highly porous whisker-structured mullite ceramic membrane for simulated oil-in-water emulsion wastewater treatment. ACS Sustain. Chem. Eng. 4 (4), 2098–2106.

Dickhout, J., Lammertink, R., de Vos, W., 2019. Membrane filtration of anionic surfactant stabilized emulsions: effect of ionic strength on fouling and droplet adhesion. Colloids Interfaces 3 (1).

Dickhout, J.M., Moreno, J., Biesheuvel, P.M., Boels, L., Lammertink, R.G.H., de Vos, W. M., 2017. Produced water treatment by membranes: a review from a colloidal perspective. J. Colloid Interface Sci. 487, 523–534.

Dobson, K.D., Roddick-Lanzilotta, A.D., McQuillan, A.J., 2000. An in situ infrared spectroscopic investigation of adsorption of sodium dodecylsulfate and of cetyltrimethylammonium bromide surfactants to TiO₂, ZrO₂, Al₂O₃, and Ta₂O₅ particle films from aqueous solutions. Vib. Spectrosc 24 (2), 287–295.

Dong, B.-B., Wang, F.-H., Yang, M.-Y., Yu, J.-L., Hao, L.-Y., Xu, X., Wang, G., Agathopoulos, S., 2019. Polymer-derived porous SiOC ceramic membranes for efficient oil-water separation and membrane distillation. J. Membr. Sci. 579, 111–119.

Ebrahimi, M., Willershausen, D., Ashaghi, K.S., Engel, L., Placido, L., Mund, P., Bolduan, P., Czermak, P., 2010. Investigations on the use of different ceramic membranes for efficient oil-field produced water treatment. Desalination 250 (3), 991–996.

Eray, E., Candelario, V.M., Boffa, V., Safafar, H., Østedgaard-Munck, D.N., Zahrtmann, N., Kadrispahic, H., Jørgensen, M.K., 2021. A roadmap for the development and applications of silicon carbide membranes for liquid filtration: recent advancements, challenges, and perspectives. Chem. Eng. J. 414, 128826.

Fernández, E., Benito, J.M., Pazos, C., Coca, J., 2005. Ceramic membrane ultrafiltration of anionic and nonionic surfactant solutions. J. Membr. Sci. 246 (1), 1–6.

Fraga, M.C., Sanches, S., Crespo, J.G., Pereira, V.J., 2017. Assessment of a new silicon carbide tubular honeycomb membrane for treatment of olive mill wastewaters. Membranes (Basel) 7 (1).

Fux, G., Ramon, G.Z., 2017. Microscale dynamics of oil droplets at a membrane surface: deformation, reversibility, and implications for fouling. Environ. Sci. Technol. 51 (23), 13842–13849.

Gu, T., Zhu, B.-Y., 1990. The S-type isotherm equation for adsorption of nonionic surfactants at the silica gel—Water interface. Colloids Surf 44, 81–87.

He, C., Vidic, R.D., 2016. Application of microfiltration for the treatment of Marcellus Shale flowback water: influence of floc breakage on membrane fouling. J. Membr. Sci. 510, 348–354.

He, Z., Kasemset, S., Kirschner, A.Y., Cheng, Y.H., Paul, D.R., Freeman, B.D., 2017. The effects of salt concentration and foulant surface charge on hydrocarbon fouling of a poly(vinylidene fluoride) microfiltration membrane. Water Res 117, 230–241.

Hofs, B., Ogier, J., Vries, D., Beerendonk, E.F., Cornelissen, E.R., 2011. Comparison of ceramic and polymeric membrane permeability and fouling using surface water. Sep. Purif. Technol. 79 (3), 365–374.

Hong, S., Elimelech, M., 1997. Chemical and physical aspects of natural organic matter (NOM) fouling of nanofiltration membranes. J. Membr. Sci. 132 (2), 159–181.

Hua, F.L., Tsang, Y.F., Wang, Y.J., Chan, S.Y., Chua, H., Sin, S.N., 2007. Performance study of ceramic microfiltration membrane for oily wastewater treatment. Chem. Eng. J. 128 (2–3), 169–175.

Kasemset, S., He, Z., Miller, D.J., Freeman, B.D., Sharma, M.M., 2016. Effect of polydopamine deposition conditions on polysulfone ultrafiltration membrane properties and threshold flux during oil/water emulsion filtration. Polymer (Guildf) 97, 247–257.

Kosmulski, M., 2011. The pH-dependent surface charging and points of zero charge: V. Update. J. Colloid Interface Sci. 353 (1), 1–15.

Kouchaki Shalmani, A., ElSherbiny, I.M.A., Panglisch, S., 2020. Application-oriented mini-plant experiments using non-conventional model foulants to evaluate new hollow fiber membrane materials. Sep. Purif. Technol. 251, 117345.

Lee, S.-J., Kim, J.-H., 2014. Differential natural organic matter fouling of ceramic versus polymeric ultrafiltration membranes. Water Res 48, 43–51.

Lehman, S.G., Liu, L., 2009. Application of ceramic membranes with pre-ozonation for treatment of secondary wastewater effluent. Water Res 43 (7), 2020–2028.

Lin, Y.-M., Rutledge, G.C., 2018. Separation of oil-in-water emulsions stabilized by different types of surfactants using electrospun fiber membranes. J. Membr. Sci. 563, 247–258.

Lin, Y.M., Song, C., Rutledge, G.C., 2019. Functionalization of Electrospun Membranes with Polyelectrolytes for Separation of Oil-In-Water Emulsions. Adv. Mater. Interfaces 6 (23), 1901285.

Lu, D., Zhang, T., Gutierrez, L., Ma, J., Croué, J.-P., 2016. Influence of surface properties of filtration-layer metal oxide on ceramic membrane fouling during ultrafiltration of oil/water emulsions. Environ. Sci. Technol. 50 (9), 4668–4674.

Lu, D.W., Zhang, T., Ma, J., 2015. Ceramic Membrane fouling during ultrafiltration of Oil/Water Emulsions: roles played by stabilization surfactants of oil droplets. Environ. Sci. Technol. 49 (7), 4235–4244.

Luo, J., Ding, L., Wan, Y., Jaffrin, M.Y., 2012. Threshold flux for shear-enhanced nanofiltration: experimental observation in dairy wastewater treatment. J. Membr. Sci. 409-410, 276–284.

Matos, M., Gutiérrez, G., Lobo, A., Coca, J., Pazos, C., Benito, J.M., 2016. Surfactant effect on the ultrafiltration of oil-in-water emulsions using ceramic membranes. J. Membr. Sci. 520, 749–759.

Miller, D.J., Kasemset, S., Paul, D.R., Freeman, B.D., 2014a. Comparison of membrane fouling at constant flux and constant transmembrane pressure conditions. J. Membr. Sci. 454, 505–515.

Miller, D.J., Kasemset, S., Wang, L., Paul, D.R., Freeman, B.D., 2014b. Constant flux crossflow filtration evaluation of surface-modified fouling-resistant membranes. J. Membr. Sci. 452, 171–183.

Morana, B., Pandraud, G., Creemer, J.F., Sarro, P.M., 2013. Characterization of LPCVD amorphous silicon carbide (a-SiC) as material for electron transparent windows. Mater. Chem. Phys. 139 (2), 654–662.

Nagasawa, H., Omura, T., Asai, T., Kanezashi, M., Tsuru, T., 2020. Filtration of surfactant-stabilized oil-in-water emulsions with porous ceramic membranes: effects of membrane pore size and surface charge on fouling behavior. J. Membr. Sci. 610, 118210.

Nguyen, L.A.T., Schwarze, M., Schomäcker, R., 2015. Adsorption of non-ionic surfactant from aqueous solution onto various ultrafiltration membranes. J. Membr. Sci. 493, 120–133.

Panpanit, S., Visvanathan, C., Muttamara, S., 2000. Separation of oil–water emulsion from car washes. Water Sci. Technol. 41 (10–11), 109–116.

Sammalkorpi, M., Karttunen, M., Haataja, M., 2009. Ionic surfactant aggregates in saline solutions: sodium dodecyl sulfate (SDS) in the presence of excess sodium chloride (NaCl) or calcium chloride (CaCl₂). J. Phys. Chem. B 113 (17), 5863–5870.

Shi, Y., Zheng, Q., Ding, L., Yang, F., Jin, W., Tang, C.Y., Dong, Y., 2022. Electro-enhanced separation of microsized oil-in-water emulsions via metallic membranes: performance and mechanistic insights. Environ. Sci. Technol. https://doi.org/10.1021/acs.est.2c00336.

Tanudjaja, H.J., Tarabara, V.V., Fane, A.G., Chew, J.W., 2017. Effect of cross-flow velocity, oil concentration and salinity on the critical flux of an oil-in-water emulsion in microfiltration. J. Membr. Sci. 530, 11–19.

Trinh, T.A., Han, Q., Ma, Y., Chew, J.W., 2019. Microfiltration of oil emulsions stabilized by different surfactants. J. Membr. Sci. 579, 199–209.

Tummons, E.N., Chew, J.W., Fane, A.G., Tarabara, V.V., 2017. Ultrafiltration of saline oil-in-water emulsions stabilized by an anionic surfactant: effect of surfactant concentration and divalent counterions. J. Membr. Sci. 537, 384–395.

Virga, E., Bos, B., Biesheuvel, P.M., Nijmeijer, A., de Vos, W.M., 2020. Surfactant-dependent critical interfacial tension in silicon carbide membranes for produced water treatment. J. Colloid Interface Sci. 571, 222–231.

Vroman, T., Beaume, F., Armanges, V., Gout, E., Remigy, J.-C.J.J.o.M.S., 2020. Critical backwash flux for high backwash efficiency: case of ultrafiltration of bentonite suspensions. J. Membr. Sci. 620, 118836.

Wang, X., Sun, K., Zhang, G., Yang, F., Lin, S., Dong, Y., 2022. Robust zirconia ceramic membrane with exceptional performance for purifying nano-emulsion oily wastewater. Water Res 208, 117859.

Wenzlick, M., Siefert, N., 2020. Techno-economic analysis of converting oil & gas produced water into valuable resources. Desalination 481, 114381.

Wu, H., Sun, C., Huang, Y., Zheng, X., Zhao, M., Gray, S., Dong, Y., 2022. Treatment of oily wastewaters by highly porous whisker-constructed ceramic membranes: separation performance and fouling models. Water Res 211, 118042.

Xu, M., Xu, C., Rakesh, K.P., Cui, Y., Yin, J., Chen, C., Wang, S., Chen, B., Zhu, L., 2020. Hydrophilic SiC hollow fiber membranes for low fouling separation of oil-in-water emulsions with high flux. RSC Adv 10 (8), 4832–4839.

Yang, M., Hadi, P., Yin, X., Yu, J., Huang, X., Ma, H., Walker, H., Hsiao, B.S., 2021. Antifouling nanocellulose membranes: how subtle adjustment of surface charge lead to self-cleaning property. J. Membr. Sci. 618, 118739.

Zhang, D.-S., Abadikhah, H., Wang, J.-W., Hao, L.-Y., Xu, X., Agathopoulos, S., 2019. β-SiAlON ceramic membranes modified with SiO₂ nanoparticles with high rejection rate in oil-water emulsion separation. Ceram. Int. 45 (4), 4237–4242.

Zhang, Q., Fan, Y., Xu, N., 2009. Effect of the surface properties on filtration performance of Al₂O₃–TiO₂ composite membrane. Sep. Purif. Technol. 66 (2), 306–312.

Zhu, L., Chen, M.L., Dong, Y.C., Tang, C.Y.Y., Huang, A.S., Li, L.L., 2016. A low-cost mullite-titania composite ceramic hollow fiber microfiltration membrane for highly efficient separation of oil-in-water emulsion. Water Res 90, 277–285.

Zhu, X.B., Dudchenko, A., Gu, X.T., Jassby, D., 2017. Surfactant-stabilized oil separation from water using ultrafiltration and nanofiltration. J. Membr. Sci. 529, 159–169.

Zsirai, T., Qiblawey, H., Buzatu, P., Al-Marri, M., Judd, S.J., 2018. Cleaning of ceramic membranes for produced water filtration. J. Petrol. Sci. Eng. 166, 283–289.